Atmos. Chem. Phys. Discuss., 14, 3269–3300, 2014
www.atmos-chem-phys-discuss.net/14/3269/2014/
doi:10.5194/acpd-14-3269-2014

Atmospheric Chemistry and Physics
Discussions
Open Access

Impacts of the East Asian summer monsoon on interannual variations of summertime surface-layer ozone concentrations over China

Y. Yang[1,2], H. Liao[1], and J. Li[3]

[1]State Key Laboratory of Atmospheric Boundary Layer Physics and Atmospheric Chemistry, Institute of Atmospheric Physics, Chinese Academy of Sciences, Beijing, China
[2]Graduate University of Chinese Academy of Science, Beijing, China
[3]State Key Laboratory of Numerical Modeling for Atmospheric Sciences and Geophysical Fluid Dynamics, Institute of Atmospheric Physics, Chinese Academy of Sciences, Beijing, China

Received: 25 November 2013 – Accepted: 17 January 2014 – Published: 4 February 2014

Correspondence to: H. Liao (hongliao@mail.iap.ac.cn)

Published by Copernicus Publications on behalf of the European Geosciences Union.

Abstract

We apply a global three-dimensional Goddard Earth Observing System (GEOS) chemical transport model (GEOS-Chem) driven by NASA/GEOS-4 assimilated meteorological fields to quantify the impacts of the East Asian summer monsoon (EASM) on interannual variations of summertime surface-layer O_3 concentrations over China. With anthropogenic emissions fixed at year 2005 levels, model simulation for years 1986–2006 shows that the changes in meteorological parameters alone lead to interannual variations in surface-layer O_3 concentrations by 2–5 % over central eastern China, 1–3 % in northwestern China, and 5–10 % over the Tibetan Plateau as well as the border and coastal areas of South China, as the interannual variations are relative to the average O_3 concentrations over the 21 yr. Over 1986–2006, O_3 concentration averaged over the whole China is found to correlate positively with the EASM index with a large correlation coefficient of +0.75, indicating that JJA O_3 concentrations are lower (or higher) in weaker (or stronger) EASM years. Relative to JJA surface-layer O_3 concentrations in the strongest EASM years (1990, 1994, 1997, 2002, and 2006), O_3 levels in the weakest EASM years (1988, 1989, 1996, 1998, and 2003) are lower over almost whole China with a nation mean lower O_3 concentration by 2.0 ppbv (or 4 %). Regionally, the largest percentage differences in O_3 concentration between the weakest and strongest EASM years are found to exceed 6 % in northeastern China, southwestern China, and over the Tibetan Plateau. Sensitivity studies show that the difference in transboundary transport of O_3 is the most dominant factor that leads to lower O_3 concentrations in the weakest EASM years than in the strongest EASM years, which, together with the enhanced vertical convections in the weakest EASM years, explain about 80 % of the differences in surface-layer O_3 concentrations between the weakest and strongest EASM years. We also find that the changes in the EASM strength are as important as the changes in anthropogenic emissions over 1986–2006 in influencing JJA surface-layer O_3 concentrations in China.

1 Introduction

Tropospheric O_3 is an air pollutant harmful to human health and ecosystems (Shindell et al., 2012). It is also (after CO_2 and CH_4) the third most important contributor to greenhouse effect (Intergovernmental Panel on Climate Change (IPCC), 2007). High O_3 concentrations have been observed in many Chinese sites, with seasonal mean concentrations of 20–60 ppbv (Yan et al., 1997, 2003; H. X. Wang et al., 2005; T. Wang et al., 2009; Y. Wang et al., 2011; Takami et al., 2006; Tu et al., 2007; Lin et al., 2008; Yang et al., 2008; Zhang et al., 2008) and episodic concentrations of exceeding 100 ppbv (T. Wang et al., 2006; Z. F. Wang et al., 2006; Duan et al., 2008). Concentrations of O_3 are driven by a combination of precursor emissions and the regional meteorological conditions.

Meteorological parameters in summer in eastern China vary with the East Asian summer monsoon (EASM). The EASM prevails in May–September every year, with strong southerlies bringing clean, warm, and moist air from the oceans to eastern China and rain belts that stretch for thousands of kilometers in the west–east direction in eastern China (Tao and Chen, 1987; Wang and Ding, 2008). Previous observational and modeling studies have shown that such patterns of winds and precipitation of the EASM influence the seasonal variations of O_3 in China (Chan et al., 1998; Li et al., 2007; He et al., 2008; Wang et al., 2011) and in the west Pacific region (Pochanart et al., 2002; Tanimoto et al., 2005; Yamaji et al., 2006). He et al. (2008) analyzed the seasonal variations of O_3 concentrations measured over 2004–2006 and found that O_3 concentrations peak in spring and autumn with a summer trough in central eastern China and the west Pacific, the areas that are influenced by clean air from the southern oceans during the summer monsoon. Studies by Wang et al. (2008), Lin et al. (2009), and Zhao et al. (2010) reported that the increasing clouds associated with the EASM rainfall suppress photochemical production of O_3 by altering solar radiation, which also contribute to the minimum O_3 concentrations in summer.

The strength of the EASM exhibits large interannual variations as a result of the interactions between the atmosphere and oceans (Webster et al., 1998). No previous studies, to our knowledge, have systematically examined the impacts of the EASM on interannual variations of summertime O_3 in China. Recently, Zhou et al. (2013) analyzed 2000–2010 ozonesonde data from Hong Kong and found a close link between lower tropospheric O_3 and the East Asian monsoon on interannual scales, but their analyses were focused on O_3 in Hong Kong in spring and autumn. We present here a study to examine the impacts of the EASM on interannual variations of summertime surface-layer O_3 concentrations over China, based on 1986–2006 simulations of O_3 concentrations using the global chemical transport model GEOS-Chem driven by the assimilated meteorological fields. This work is a companion study to the work of Zhu et al. (2012), which investigated the impacts of the EASM on interannual to decadal variations of summertime aerosols in China.

The GEOS-Chem model and numerical experiments are described in Sect. 2. Section 3 presents simulated interannual variations of summertime O_3 in China. Section 4 shows simulated impacts of the EASM on interannual variations of summertime O_3, and Sect. 5 examines the mechanisms through which the EASM influences the interannual variations. Section 6 compares the impacts of changing monsoon strength with those of changing anthropogenic emissions on O_3 concentrations in China.

2 Model description and experimental design

2.1 GEOS-Chem model

We simulate tropospheric O_3 using the global chemical transport model GEOS-Chem (version 8.2.1, http://acmg.seas.harvard.edu/geos) driven by the assimilated meteorological fields from the Goddard Earth Observing System (GEOS) of the NASA Global Modeling and Assimilation Office (GMAO). The version of the model used here has a horizontal resolution of 2° latitude by 2.5° longitude and 30 vertical layers from the surface to 0.01 hPa. The GEOS-Chem model includes a fully coupled treatment of tropospheric O_3-NO_x-VOC chemistry and aerosol components. Tropospheric O_3 is simulated with about 80 species and over 300 chemical reactions (Bey et al., 2001). Photolysis rates are computed using the Fast-J algorithm (Wild et al., 2000). The cross-tropopause O_3 flux in this version of GEOS-Chem is specified with the synthetic ozone ("Synoz") method (McLinden et al., 2000) as implemented by Bey et al. (2001), which includes a passive, ozone-like tracer released into the stratosphere at a constant rate equivalent to that of the prescribed cross-tropopause ozone flux of 499 Tg O_3 yr^{-1}.

2.2 Emissions

Global emissions of O_3 precursors, aerosol precursors, and aerosols in the GEOS-Chem model follow Park et al. (2003, 2004), but anthropogenic emissions of NO_x, CO, SO_2, and NH_3 over East Asia are overwritten by the emissions inventory of Streets et al. (2003). Global anthropogenic emissions of nonmethane hydrocarbons are from the GEIA inventory (Piccot et al., 1992). Biomass burning emissions are taken from the GFED-2 inventory (van der Werf et al., 2006). These inventories are then scaled for 2005 on the basis of economic data and energy statistics as described by van Donkelaar et al. (2008). The biogenic emissions in the GEOS-Chem model are simulated using the MEGAN module (Guenther et al., 2006; Wiedinmyer et al., 2007). Soil NO_x emissions are computed using a modified version of the algorithm proposed by Yienger and Levy (1995). Lightning emissions follow Price and Rind (1992), with the NO_x vertical profile proposed by Pickering et al. (1998).

The simulations of tropospheric O_3 by the GEOS-Chem model have been evaluated in previous studies for the United States (Fiore et al., 2005; Wu et al., 2008; Wang et al., 2009) and China (Wang et al., 2008, 2011; Jeong and Park, 2013; Lou and Liao, 2014). The model was found to be able to capture the magnitude and spatial distribution of O_3 in China.

Title Page
Abstract Introduction
Conclusions References
Tables Figures
◀ ▶
Back Close
Full Screen / Esc
Printer-friendly Version
Interactive Discussion

2.3 Experiments

In this study concentrations of O_3 in China for years 1986–2006 are simulated driven by the GEOS-4 meteorological fields. To identify the key processes that influence O_3 concentrations in different monsoon years, we perform the following simulations:

1. O3_TOT: the standard simulation of O_3 concentrations for years 1986–2006. Global anthropogenic and biomass burning emissions of NO_x, CO, nonmethane hydrocarbons, aerosols and aerosol precursors are fixed at year 2005 levels. Meteorological fields are allowed to vary over 1986–2006. The cross-tropopause O_3 flux is set to 499 $\text{Tg}\,\text{yr}^{-1}$ using the "Synoz" scheme.
2. O3_TB: the sensitivity simulation of O_3 concentrations for years 1986–2006 to quantify the role of transboundary transport of O_3 in different monsoon years. The model setups are the same as those in O3_TOT except that all natural and anthropogenic emissions in China are turned off.
3. O3_ST: the sensitivity simulation of O_3 concentrations for years 1986–2006 to quantify the impact of cross-tropopause O_3 flux on surface-layer O_3 concentrations. The model setups are the same as those in O3_TOT except that natural and anthropogenic emissions are turned off globally.
4. O3_EMIS: the sensitivity simulations to compare the impacts of changing anthropogenic emissions with those of changing monsoon strength. Two sensitivity simulations are conducted with 1986 and 2006 anthropogenic emissions, respectively. The emissions in year 1986 are simulated using the default scaling factors in the model (van Donkelaar et al., 2008). Year 2006 meteorological parameters are used to drive both simulations. The cross-tropopause O_3 flux is set to 499 $\text{Tg}\,\text{yr}^{-1}$ using the "Synoz" scheme.

2.4 East Asian summer monsoon index

The interannual variations in strength of the EASM are commonly represented by the EASM index (EASMI). The EASMI introduced by Li and Zeng (2002) is used in this study. The formulation for calculating EASMI based on the GEOS-4 meteorological parameters was given in Zhu et al. (2012). Positive values of EASMI indicate strong monsoon years whereas negative values indicate weak monsoon years. Physically, a strong summer monsoon in China is characterized by strong southerlies extending from southern China to northern China, a deficit of rainfall in the middle and lower reaches of the Yangtze River, and large rainfall in northern China. On the contrary, in a weak summer monsoon year, China experiences weak southerlies, large rainfall in southern China, and a deficit of rainfall in northern China. The movement of the rain belts is associated with the strength of the southerlies.

3 Simulated interannul variations of summertime O_3 in China

Figure 1a shows the simulated spatial distribution of June-July-August (JJA) surface-layer O_3 concentrations averaged over 1986–2006 from the O_3_TOT simulation. Over eastern China, simulated O_3 concentrations are 50–65 ppbv in northern China and 25–50 ppbv in southern China. Such pattern of higher O_3 concentrations in northern China than in southern China results from that the strong southerlies bring clean air from the oceans to southern China during the summer monsoon season (Chan et al., 1998; Yamaji et al., 2006; Li et al., 2007; He et al., 2008; Wang et al., 2011). In western China, simulated O_3 exhibits maximum concentrations of 65 ppbv owing to large transboundary transport by westerlies and downward transport from the stratosphere, which will be discussed further in Sect. 5.

The interannual variations in simulated JJA O_3 concentrations can be quantified by mean absolute deviation (MAD) and absolute percent departure from the mean (APDM) defined as $\mathrm{MAD} = \frac{1}{n}\sum_{i=1}^{n}\left|P_i - \frac{1}{n}\sum_{i=1}^{n}P_i\right|$ and $\mathrm{APDM} = 100\,\% \times$

MAD/$\left(\frac{1}{n}\sum_{i=1}^{n}P_i\right)$, where P_i is the simulated JJA mean O_3 concentration of year i, and n is the number of years examined ($n = 21$ for years 1986–2006). Therefore MAD represents the absolute interannual variation and APDM represents the interannual variation relative to the average of O_3 concentration over the n years. The MAD values of JJA surface-layer O_3 concentrations (Fig. 1b) are 1.0–4.0 ppbv in China, with the largest values of exceeding 2 ppbv found over northeastern China, coastal areas of South China, and the Tibetan Plateau. As shown in Fig. 1c, the APDM values are in the range of 2–5 % over central eastern China where summer monsoon prevails, 1–3 % in northwestern China, and 5–10 % over the Tibetan Plateau as well as the border and coastal areas of South China. These interannual variations in O_3 are significant as compared to the impacts of reductions in emissions of O_3 precursors. Han et al. (2005) showed by modeling studies that, in eastern China, reductions in NO_x or total VOCs (anthropogenic plus biogenic VOCs) by 50 % lead to changes in JJA O_3 concentrations by 10–20 %.

Because of the lack of long-term O_3 measurements in China, we evaluate the simulated interannual variations of JJA surface-layer O_3 concentrations at two sites (Fig. 2): Hok Tsui in Hong Kong (22°13′ N, 114°15′ E) and Ryori in Japan (39°03′ N, 144°82′ E). The measurements at Hok Tsui are taken from Wang et al. (2009b), and those at Ryori site are from the WMO World Data Center for Greenhouse Gases (WDCGG, http://ds.data.jma.go.jp/gmd/wdcgg/). At Hok Tsui, simulated O_3 concentrations are higher than the observations in JJA. This discrepancy may due to the model's overestimate of O_3 in marine boundary layers in summer (Liu et al., 2006). Interannually, the model captures well the peaks and troughs of the observed JJA O_3 concentrations, with a high correlation coefficient of +0.87. The model underestimates JJA O_3 concentrations at Ryori, probably due to the uncertainties with local emissions, but captures mostly the years with maximum or minimum O_3 levels with a correlation coefficient of +0.47. The simulated APDM values at Hok Tsui and Ryori are both 7 %, smaller than the observed interannual variations of 22 % and 8 % at these two sites, respectively, which can be attributed to the fixed anthropogenic emissions of O_3 precursors in our O3_TOT simulation.

4 Impacts of the EASM on interannual variations of summertime O_3 in China

Simulated JJA surface-layer O_3 concentration averaged over the whole China is shown in Fig. 3a for years 1986–2006 based on the O_3_TOT simulation. Summertime O_3 concentrations show large interannual variations, with high (or low) O_3 concentrations in strong (or weak) monsoon years. Concentrations of O_3 are found to correlate positively with the EASMI; the correlation coefficient is +0.75 and is statistically significant at the 95th percentile. The spatial distribution of the correlation coefficients between the EASMI and O_3 concentrations from the O_3_TOT simulation is presented in Fig. 3b. Positive correlations are found in almost the whole China, and large positive correlation coefficients that exceed +0.5 are found over the region between 90° E and 110° E. Since anthropogenic emissions of O_3 precursors are kept unchanged in the simulation for 1986–2006, these strong positive correlations demonstrate that the EASM strength has large impacts on JJA O_3 concentrations over China.

In order to quantify the impacts of the EASM on O_3 concentrations over China, we show in Fig. 4a and b, respectively, the absolute and percentage differences between O_3 concentrations averaged over five weakest EASM years (1988, 1989, 1996, 1998, and 2003) and those averaged over five strongest EASM years (1990, 1994, 1997, 2002, and 2006). These weakest (or strongest) monsoon years are selected within 1986–2006 based on the five largest negative (or positive) values of the normalized EASMI as shown in Fig. 3a. Relative to the concentrations in the strongest monsoon years, O_3 levels in the weakest monsoon years are lower over almost the whole China, with the largest reductions of exceeding 3 ppbv (or 6 %) in northeastern and southwestern China and over or near the Tibetan Plateau. Concentrations of O_3 in the weakest monsoon years are simulated to be higher than those in the strongest monsoon years by 3–5 ppbv (or 6–15 %) over the East China Sea. The pattern of the differences in

O_3 concentrations agrees with the spatial distribution of the correlation coefficients (Fig. 3b). Averaged over China, O_3 level in the weakest monsoon years is lower than that in the strongest monsoon years by 2.0 ppbv (or 4 %).

Figure 4c and d is a pressure-longitude plot of the differences in O_3 averaged over the latitude range of 20–46° N. From the surface to 250 hPa altitude, O_3 levels in the weakest monsoon years are lower by up to 5 ppbv (or 8 %) over 80–115° E and are higher by 1–3 ppbv (or 3–6 %) over 120–135° E relative to the concentrations in the strongest monsoon years. Concentrations of O_3 at 130–250 hPa altitudes exhibit increases in the weakest monsoon years, with maximum increases of 4–7 ppbv (3–6 %) over 80° E and 130° E, as a result of the anomalous horizontal convergence at these layers.

5 Mechanisms of the impacts of the EASM on summertime O_3

5.1 Impacts of the EASM on transboundary transport of O_3

Considering that O_3 concentrations in almost whole China are lower in the weakest monsoon years than in the strongest monsoon years and that tropospheric O_3 has a relatively long lifetime of 3–4 weeks (Seinfeld and Pandis, 2006), we examine firstly the impacts of the EASM on transboundary transport of O_3. Figure 5 shows JJA horizontal winds at 850 hPa and 500 hPa averaged over 1986–2006 as well as the composite differences in JJA horizontal winds between the five weakest and five strongest EASM years at these two layers. In JJA, prevailing southerlies can be seen in southeastern China in the lower and middle troposphere (Fig. 5a and b), which are the typical features in winds during the EASM. In JJA, relative to the strongest monsoon years, anomalous southerlies are found in southern China and anomalous westerlies are found in southeastern China in the weakest monsoon years (Fig. 5c and d), which agree with the anomalous winds between weak and strong monsoon years reported in Li and Zeng (2002) and Huang (2004).

The differences in winds in different monsoon years lead to differences in transboundary transport of O_3. We show in Fig. 6 the differences in simulated horizontal mass fluxes of O_3 at the four lateral boundaries of the selected box of (85–120° E, 20–46° N, the surface to 250 hPa) and in Table 1 the summary of the composite analysis on fluxes of O_3 in and out of this box, based on simulation O3_TOT. This box is selected to capture the features of transboundary O_3 transport that influence O_3 concentrations in China. The location of the box is shown in Fig. 5d. Relative to the strongest monsoon years, the weakest monsoon years have less inflow by 0.1 Tg at the west boundary, larger inflow fluxes of O_3 by 4.2 Tg at the south boundary and by 5.5 Tg at the north boundary, and larger outflow by 12.9 Tg at the east boundary (Table 1 and Fig. 6), as mass fluxes are summed over JJA. The net effect is a larger transboundary outflow of O_3 by 3.3 Tg in the weakest monsoon years than in the strongest monsoon years. The anomalous westerlies in southeastern China are especially important, which bring polluted air with high O_3 concentrations to the coastal areas and the East China Sea (Fig. 6d), leading to reductions in O_3 concentration in China.

The role of changes in transboundary transport of O_3 can be further quantified by the simulation O3_TB with natural and anthropogenic emissions of O_3 precursors in China turned off. The spatial distribution of O_3 from simulation O3_TB (referred to as TBO_3 hereafter) is presented in Fig. 7a. TBO_3 concentrations show a distinct spatial gradient over China, decreasing from about 55 ppbv in northwestern China to about 10 ppbv in southeastern China. The JJA TBO_3 concentration averaged over the whole China is 30 ppbv, which is about 62 % of the average concentration simulated in O3_TOT, indicating that a significant fraction of surface-layer O_3 over China is from transboundary transport. The differences in TBO_3 concentrations between the weakest and strongest monsoon years (Fig. 7d) are, to a large extent, similar to those from simulation O3_TOT (Fig. 4a), in terms of both distributions and magnitudes. Averaged over China, the difference in TBO_3 between the weakest and strongest monsoon years is −1.6 ppbv, which accounts for 80 % of the corresponding difference obtained in O3_TOT. The JJA mass fluxes of TBO3 for the selected box of (85–120° E, 20–46° N, the surface to 250 hPa) are also similar to those simulated in O3_TOT (Table 1), with a net horizontal outflow of 2.8 Tg. These model results indicate that the differences in transboundary transport of O_3 is a dominant mechanism through which the EASM influences interannual variations of JJA O_3 concentrations in China.

5.2 Impacts of the EASM on vertical transport of O_3

Vertical circulations in China have some unique features during the EASM. In summer, two major ascending branches of winds (or strong convections) are observed throughout the entire troposphere (Fig. 8a). One branch is located over the Yangtze River valley, associated with the Mei-yu front (rain belt) of the EASM (Ding and Chan, 2005). The other branch is over the Tibetan Plateau, because the Tibetan Plateau during summer serves as a large heat source, which uplifts heated air to the upper troposphere and even to the stratosphere (Ye, 1981). Figure 8a shows JJA vertical velocity and simulated vertical mass flux of O_3 at 500 hPa averaged over 1986–2006. Since vertical velocity is not available from the reanalyzed GEOS-4 meteorological fields, vertical winds presented here are from the NCEP/NACR reanalysis data. The simulated mass fluxes are obtained in O3_TOT. The largest vertical mass fluxes of O_3 are simulated to occur over northern China and western China where surface-layer O_3 concentrations are high, and to occur over the Tibetan Plateau and its surrounding areas as a result of the strong convections here.

Figure 8b shows the differences in JJA vertical wind velocity and simulated vertical mass flux of O_3 at 500 hPa between the weakest and strongest monsoon years. Relative to the strongest monsoon years, anomalous convections are found over central and western China in the weakest monsoon years, leading to enhanced upward transport of O_3 from the surface to upper troposphere at these locations. The differences in vertical winds shown in Fig. 8b agree with those reported in Huang (2004).

Table 1 also summarizes the composite analysis on vertical fluxes of O_3 through the top side of the selected box (85–120° E, 20–46° N, the surface to 250 hPa). In simulation O3_TOT, the upward flux of O_3 through the top plane of the box in the weakest monsoon years is larger than that in the strongest monsoon years by 1.4 Tg. This anomalous vertical outflow of 1.4 Tg is smaller than the anomalous horizontal transboundary outflow of 3.3 Tg (Sect. 5.1), indicating that the differences in vertical transport of O_3 also contribute to lower JJA O_3 concentrations in China in the weakest monsoon years than in the strongest monsoon years, but the impact of the differences in vertical transport is smaller than that of the differences in transboundary transport of O_3.

5.3 Impact of cross-tropopause transport on surface-layer O_3 concentrations

The cross-tropopause transport of O_3 from the stratosphere is an important source of tropospheric O_3. Simulation O_3_ST is performed to quantify the impact of cross-tropopause transport on JJA surface-layer O_3 concentrations. The simulated JJA concentrations of O_3 in simulation O_3_ST (referred to as STO_3) at the surface-layer averaged over 1986–2006 are presented in Fig. 7b. STO_3 shows maximum concentrations of 15–20 ppbv over northwestern China, contributing to the high O_3 concentrations in western China simulated in O3_TOT. Averaged over China, the surface-layer concentration of JJA STO_3 is 8 ppbv, which is about 17 % of that of JJA O_3 simulated in O3_TOT. Concentrations of STO_3 increase with altitude; the ratio of STO_3 to O_3 simulated in O3_TOT is about 50 % at 200 hPa and about 80 % at 100 hPa. Figure 7e shows the differences in surface-layer STO_3 concentrations between the weakest and strongest monsoon years. Relative to the strongest monsoon years, surface-layer STO_3 concentrations are lower by 1–2 ppbv over central China and the Tibetan Plateau in the weakest monsoon years. Averaged over China, the difference in STO_3 between the weakest and strongest monsoon years is −0.45 ppbv, which only accounts for 23 % of the corresponding difference in $TOTO_3$ and hence indicates that the variations in O_3 transported from the stratosphere in different monsoon years are not the major factors that drive the interannual variations of JJA surface-layer O_3 concentrations in China. Note that the cross-tropopause O_3 flux in O3_TOT and O3_ST is specified with the synthetic ozone ("Synoz") method (McLinden et al., 2000) with a constant cross-tropopause ozone flux of 499 Tg $O_3\,yr^{-1}$. The latest version of the GEOS-Chem model also has an option of using the linearized ozone ("Linoz") parameterization scheme of McLinden et al. (2000) to represent O_3 in the stratosphere, in which the ozone vertical profiles across the tropopause are relaxed back toward climatological profiles and hence cross-tropopause O_3 flux varies with time step and location. We have tested using "Linoz" instead of "Synoz" and found that these two schemes obtain same conclusion about the impact of cross-tropopause O_3 on JJA surface-layer O_3 in China.

5.4 Impacts of the EASM on local chemical production of O_3

The differences in O_3 concentrations between O_3_TOT and O_3_TB simulations are attributed to the enhancement of O_3 due to Chinese emissions, referred to as Chinese local O_3 ($LOCO_3$). Figure 8c shows that high concentrations of $LOCO_3$ are located in eastern China where the emissions of O_3 precursors are large. The maximum $LOCO_3$ concentrations reach 40–45 ppbv. The $LOCO_3$ concentration averaged over the whole China is 18 ppbv, which is about 38 % of the value simulated in O3_TOT. Figure 8f presents the differences in simulated $LOCO_3$ between the weakest and strongest EASM years. Relative to the strongest monsoon years, $LOCO_3$ concentrations in the weakest monsoon years are lower by 2–5 ppbv over southern China and slightly higher by up to 1 ppbv over central China. Averaged over China, the difference in $LOCO_3$ between the weakest and strongest monsoon years is −0.4 ppbv, which accounts for 20 % of the corresponding difference in $TOTO_3$ and hence reflects the small impacts of monsoon strength on local chemical production of O_3.

The small impacts of monsoon strength on local chemical production of O_3 can be further justified by examining the net chemical production of O_3 within the selected box (85–120° E, 20–46° N, the surface to 250 hPa). Sum over the selected box, the net chemical production (chemical production – chemical loss) averaged over the weakest monsoon years is 39.0 Tg in JJA, which is smaller than that averaged over the strongest monsoon years by 0.5 %.

6 Comparison of the impact of monsoon strength with the role of changing emissions

We perform simulations O_3_EMIS to compare the impact of changing monsoon strength (Sect. 4) with that of changing anthropogenic emissions on JJA O_3 concentrations. Two sensitivity simulations are conducted with 1986 and 2006 anthropogenic emissions, respectively, and year 2006 meteorological parameters are used to drive both simulations. Relative to 1986, year 2006 emissions of NO_x, CO, and NMVOCs in China increase by 111 %, 56 %, and 9 %, respectively, leading to increases in JJA surface-layer O_3 by 9–15 ppbv in southeastern China (Fig. 9). Note the locations of large increases in O_3 here are different from those of large differences in O_3 between the weakest and strongest monsoon years (Fig. 4b). Averaged over China, the change in JJA surface-layer O_3 concentration owing to changes in emissions over 1986–2006 is +5.3 ppbv, which is larger than the difference in JJA surface-layer O_3 of 2.0 ppbv between the selected weakest and strongest monsoon years. However, the difference in surface-layer O_3 between the weak monsoon year 1998 and the strong monsoon year 1997 is −4.2 ppbv, indicating that the EASM strength can be as important as the changes in anthropogenic emission in influencing JJA O_3 concentrations in China.

7 Conclusions

We examine the impacts of the East Asian summer monsoon (EASM) on interannual variations of summertime surface-layer O_3 concentrations over China using the GEOS-Chem model driven by the assimilated GEOS-4 meteorological data. The interannual variations of O_3 concentrations are quantified by values of mean absolute deviation (MAD) and absolute percent departure from the mean (APDM), based on the simulation of O_3 for years 1986–2006 with changes in meteorological parameters but fixed anthropogenic emissions at year 2005 levels. The MAD values of JJA surface-layer O_3 concentrations in China are in the range of 1.0–4.0 ppbv, with the largest values of ex-

Title Page
Abstract Introduction
Conclusions References
Tables Figures
◂◂ ▸▸
◂ ▸
Back Close
Full Screen / Esc
Printer-friendly Version
Interactive Discussion

ceeding 2 ppbv found over northeastern China, coastal areas of South China, and the Tibetan Plateau. The APDM values of JJA surface-layer O_3 concentrations are 2–5 % over central eastern China, 1–3 % in northwestern China, and 5–10 % over the Tibetan Plateau as well as the border and coastal areas of South China.

With fixed anthropogenic emissions, simulated JJA O_3 concentrations averaged over China exhibit strong positive correlation (with a correlation coefficient of +0.75) with the East Asian summer monsoon index (EASMI) in the time period of 1986–2006, indicating that JJA O_3 concentrations are lower (or higher) in weaker (or stronger) EASM years. Relative to JJA surface-layer O_3 concentrations in the strongest EASM years (1990, 1994, 1997, 2002, and 2006), O_3 levels in the weakest EASM years (1988, 1989, 1996, 1998, and 2003) are lower over almost whole China with a nation mean lower O_3 concentration by 2.0 ppbv (or 4 %).

Sensitivity studies are performed to identify the key processes through which the variations in EASM strength influence interannual variations of JJA O_3 in China. The difference in transboundary transport of O_3 is found to be the most dominant factor that leads to lower O_3 concentrations in the weakest EASM years than in the strongest EASM years. Relative to the strongest EASM years, the weakest EASM years have less inflow by 0.11 Tg at the west boundary, larger inflow fluxes of O_3 by 4.2 Tg at the south boundary and by 5.5 Tg at the north boundary, and larger outflow by 12.9 Tg at the east boundary, as horizontal mass fluxes of O_3 at the four lateral boundaries of the selected box (85–120° E, 20–46° N, the surface to 250 hPa) are calculated. As a result, the weakest EASM years have larger outflow of O_3 than the strongest EASM years, which, together with the enhanced vertical convections in the weakest EASM years, explain about 80 % of the differences in surface-layer O_3 concentrations between the weakest and strongest EASM years.

We also perform a sensitivity simulation O_3_EMIS to compare the impact of changing monsoon strength with that of changing anthropogenic emissions on JJA O_3 concentrations. Averaged over China, the change in JJA surface-layer O_3 concentration owing to changes in emissions over 1986–2006 is +5.3 ppbv, which is larger than the difference in JJA surface-layer O_3 of 2.0 ppbv between the selected weakest and strongest monsoon years. However, for specific years, the difference in surface-layer O_3 between the weak EASM year 1998 and the strong EASM year 1997 is simulated to be −4.2 ppbv, indicating that the EASM strength is as important as the changes in anthropogenic emission in influencing JJA O_3 concentrations in China.

Acknowledgements. This work was supported by the Chinese Academy of Sciences Strategic Priority Research Program Grant No. XDA05100503, the National Natural Science Foundation of China under grants 40775083, 40825016, and 41021004, as well as the China Meteorological Administration special funding in atmospheric science GYHY200906020.

References

Bey, I., Jacob, D. J., Yantosca, Logan, R. M., J. A., Field, B. D., Fiore, A. M., Li, Q., Liu, H. Y., Mickley, L. J., and Schultz, M. G.: Global modeling of tropospheric chemistry with assimilated meteorology: model description and evaluation, J. Geophys. Res., 106, 23073–23095, doi:10.1029/2001JD000807, 2001.

Chan, L. Y., Liu, H. Y., Lam, K. S., Wang, T., Oltmans, S. J., and Harris, J. M.: Analysis of the seasonal behavior of tropospheric ozone at Hong Kong, Atmos. Environ., 32, 159–168, doi:10.1016/S1352-2310(97)00320-8, 1998.

Ding, Y. H. and Johnny, C. L. C.: The East Asian summer monsoon: an overview, Meteorol. Atmos. Phys., 89, 117–142, doi:10.1007/s00703-005-0125-z, 2005.

Duan, J. C., Tan, J. H., Yang, L., Wu, S., and Hao, J. M.: Concentration, sources and ozone formation potential of volatile organic compounds (VOCs) during ozone episode in Beijing, Atmos. Res., 88, 25–35, doi:10.1016/J.Atmosres.2007.09.004, 2008.

Fiore, A. M., Horowitz, L. W., Purves, D. W., Levy, H., Evans, M. J., Wang, Y., Li, Q., and Yantosca, R. M.: Evaluating the contribution of changes in isoprene emissions to surface ozone trends over the eastern United States, J. Geophys. Res., 110, D12303, doi:10.1029/2004JD005485, 2005.

Guenther, A., Karl, T., Harley, P., Wiedinmyer, C., Palmer, P. I., and Geron, C.: Estimates of global terrestrial isoprene emissions using MEGAN (Model of Emissions of Gases and

Aerosols from Nature), Atmos. Chem. Phys., 6, 3181–3210, doi:10.5194/acp-6-3181-2006, 2006.

Han, Z. W., Ueda, H., and Matsuda, K.: Model study of the impact of biogenic emission on regional ozone and the effectiveness of emission reduction scenarios over eastern China, Tellus B, 57, 12–27, doi:10.1111/j.1600-0889.2005.00132.x, 2005.

He, Y. J., Uno, I., Wang, Z. F., Pochanart, P., Li, J., and Akimoto, H.: Significant impact of the East Asia monsoon on ozone seasonal behavior in the boundary layer of Eastern China and the west Pacific region, Atmos. Chem. Phys., 8, 7543–7555, doi:10.5194/acp-8-7543-2008, 2008.

Huang, G.: An index measuring the interannual variation of the East Asian summer monsoon – The EAP index, Adv. Atmos. Sci., 21, 41–52, doi:10.1007/Bf02915679, 2004.

Intergovernmental Panel on Climate Change (IPCC), Climate change 2007: the physical science basis. Contribution of working group I to the fourth assessment report of the intergovernmental panel on climate change, edited by: Solomon, S. et al., Cambridge University Press, Cambridge, United Kingdom and New York, 1–996, 2007.

Jeong, J. I. and Park, R. J.: Effects of the meteorological variability on regional air quality in East Asia, Atmos. Environ., 69, 46–55, doi:10.1016/J.Atmosenv.2012.11.061, 2013.

Li, J. and Zeng, Q.: A unified monsoon index, Geophys. Res. Lett., 29, 115-1–115-4, doi:10.1029/2001GL013874, 2002.

Li, J., Wang, Z., Akimoto, H., Gao, C., Pochanart, P., and Wang, X.: Modeling study of ozone seasonal cycle in lower troposphere over east Asia, J. Geophys. Res., 112, D22S25, doi:10.1029/2006JD008209, 2007.

Lin, M., Holloway, T., Oki, T., Streets, D. G., and Richter, A.: Multi-scale model analysis of boundary layer ozone over East Asia, Atmos. Chem. Phys., 9, 3277–3301, doi:10.5194/acp-9-3277-2009, 2009.

Lin, W., Xu, X., Zhang, X., and Tang, J.: Contributions of pollutants from North China Plain to surface ozone at the Shangdianzi GAW Station, Atmos. Chem. Phys., 8, 5889–5898, doi:10.5194/acp-8-5889-2008, 2008.

Liu, X., Chance, K., Sioris, C. E., Kurosu, T. P., Spurr, R. J. D., Martin, R. V., Fu, T. M., Logan, J. A., Jacob, D. J., Palmer, P. I., Newchurch, M. J., Megretskaia, I. A., and Chatfield, R. B.: First directly retrieved global distribution of tropospheric column ozone from GOME: comparison with the GEOS-CHEM model, J. Geophys. Res., 111, D02308, doi:10.1029/2005JD006564, 2006.

Logan, J. A.: An analysis of ozonesonde data for the troposphere: recommendations for testing 3-D models and development of a gridded climatology for tropospheric ozone, J. Geophys. Res., 104, 16115–16149, doi:10.1029/1998JD100096, 1999.

Lou, S. J., Liao, H., and Zhu, B.: Impacts of aerosols on surface-layer ozone concentrations in China through heterogeneous reactions and changes in photolysis rates, Atmos. Environ., 85, 123–138, doi:10.1016/j.atmosenv.2013.12.004, 2014.

McLinden, C. A., Olsen, S. C., Hannegan, B., Wild, O., Prather, M. J., and Sundet, J.: Stratospheric ozone in 3-D models: a simple chemistry and the cross-tropopause flux, J. Geophys. Res., 105, 14653–14665, doi:10.1029/2000JD900124, 2000.

Park, R. J., Jacob, D. J., Chin, M., and Martin, R. V.: Sources of carbonaceous aerosols over the United States and implications for natural visibility, J. Geophys. Res., 108, 4355, doi:10.1029/2002JD003190, 2003.

Park, R. J., Jacob, D. J., Field, B. D., Yantosca, R. M., and Chin, M.: Natural and transboundary pollution influences on sulfate-nitrate-ammonium aerosols in the United States: implications for policy, J. Geophys. Res., 109, D15204, doi:10.1029/2003JD004473, 2004.

Piccot, S. D., Watson, J. J., and Jones, J. W.: A global inventory of volatile organic-compound emissions from anthropogenic sources, J. Geophys. Res., 97, 9897–9912, doi:10.1029/92JD00682, 1992.

Pickering, K. E., Wang, Y. S., Tao, W. K., Price, C., and Muller, J. F.: Vertical distributions of lightning NO_x for use in regional and global chemical transport models, J. Geophys. Res., 103, 31203–31216, doi:10.1029/98JD02651, 1998.

Pochanart, P., Akimoto, H., Kinjo, Y., and Tanimoto, H.: Surface ozone at four remote island sites and the preliminary assessment of the exceedances of its critical level in Japan, Atmos. Environ., 36, 4235–4250, doi:10.1016/S1352-2310(02)00339-4, 2002.

Price, C. and Rind, D.: A simple lightning parameterization for calculating global lightning distributions, J. Geophys. Res., 97, 9919–9933, doi:10.1029/92JD00719, 1992.

Sander, S. P., Friedl, R. R., DeMore, W. B., Golden, D. M., Kurylo, M. J., Hampson, R. F., Huie, R. E., Moortgat, G. K., Ravishankara, A. R., Kolb, C. E., and Molina, M. J.: Chemical Kinetics and Photochemical Data for Use in Stratospheric Modeling, Technical Report JPL Publication 00-3, Jet Propulsion Laboratory, Pasadena, CA, 2000.

Seinfeld, J. H. and Pandis, S. N.: Atmospheric Chemistry and Physics, 2nd Edn., John Wiley & Sons, Inc., Hoboken, New Jersey, 2006.

Shindell, D., Kuylenstierna, J. C. I., Vignati, E., van Dingenen, R., Amann, M., Klimont, Z., Anenberg, S. C., Muller, N., Janssens-Maenhout, G., Raes, F., Schwartz, J., Faluvegi, G., Pozzoli, L., Kupiainen, K., Höglund-Isaksson, L., Emberson, L., Streets, D., Ramanathan, V., Hicks, K., Oanh, N. T. K., Milly, G., Williams, M., Demkine, V., and Fowler, D.: Simultaneously mitigating near-term climate change and improving human health and food security, Science, 335, 183–189, doi:10.1126/science.1210026, 2012.

Streets, D. G., Bond, T. C., Carmichael, G. R., Fernandes, S. D., Fu, Q., He, D., Klimont, Z., Nelson, S. M., Tsai, N. Y., Wang, M., Woo, J. H., and Yarber, K. F.: An inventory of gaseous and primary aerosol emissions in Asia in the year 2000, J. Geophys. Res., 108, 8809, doi:10.1029/2002JD003093, 2003.

Takami, A., Wang, W., Tang, D. G., and Hatakeyama, S.: Measurements of gas and aerosol for two weeks in northern China during the winter-spring period of 2000, 2001 and 2002, Atmos. Res., 82, 688–697, doi:10.1016/J.Atmosres.2006.02.023, 2006.

Tanimoto, H., Sawa, Y., Matsueda, H., Uno, I., Ohara, T., Yamaji, K., Kurokawa, J., and Yonemura, S.: Significant latitudinal gradient in the surface ozone spring maximum over East Asia, Geophys. Res. Lett., 32, L21805, doi:10.1029/2005GL023514, 2005.

Tao, S. and Chen, L.: A Review of Recent Research on the East Asia Summer Monsoon in China, Monsoon Meteorology, Oxford University Press, Oxford, United Kingdom, 60–92, 1987.

Tu, J., Xia, Z. G., Wang, H. S., and Li, W. Q.: Temporal variations in surface ozone and its precursors and meteorological effects at an urban site in China, Atmos. Res., 85, 310–337, doi:10.1016/J.Atmosres.2007.02.003, 2007.

van der Werf, G. R., Randerson, J. T., Giglio, L., Collatz, G. J., Kasibhatla, P. S., and Arellano Jr., A. F.: Interannual variability in global biomass burning emissions from 1997 to 2004, Atmos. Chem. Phys., 6, 3423–3441, doi:10.5194/acp-6-3423-2006, 2006.

van Donkelaar, A., Martin, R. V., Leaitch, W. R., Macdonald, A. M., Walker, T. W., Streets, D. G., Zhang, Q., Dunlea, E. J., Jimenez, J. L., Dibb, J. E., Huey, L. G., Weber, R., and Andreae, M. O.: Analysis of aircraft and satellite measurements from the Intercontinental Chemical Transport Experiment (INTEX-B) to quantify long-range transport of East Asian sulfur to Canada, Atmos. Chem. Phys., 8, 2999–3014, doi:10.5194/acp-8-2999-2008, 2008.

Wang, B. and Ding, Q.: Global monsoon: dominant mode of annual variation in the tropics, Dynam. Atmos. Oceans, 44, 165–183, doi:10.1016/J.Dynatmoce.2007.05.002, 2008.

Wang, H. Q., Jacob, D. J., Le Sager, P., Streets, D. G., Park, R. J., Gilliland, A. B., and van Donkelaar, A.: Surface ozone background in the United States: Canadian and Mexican pollution influences, Atmos. Environ., 43, 1310–1319, doi:10.1016/j.atmosenv.2008.11.036, 2009.

Wang, H. X., Kiang, C. S., Tang, X. Y., Zhou, X. J., and Chameides, W. L.: Surface ozone: a likely threat to crops in Yangtze delta of China, Atmos. Environ., 39, 3843–3850, doi:10.1016/j.atmosenv.2005.02.057, 2005.

Wang, T., Ding, A., Gao, J., and Wu, W. S.: Strong ozone production in urban plumes from Beijing, China, Geophys. Res. Lett., 33, L21806, doi:10.1029/2006GL027689, 2006.

Wang, T., Wei, X. L., Ding, A. J., Poon, C. N., Lam, K. S., Li, Y. S., Chan, L. Y., and Anson, M.: Increasing surface ozone concentrations in the background atmosphere of Southern China, 1994–2007, Atmos. Chem. Phys., 9, 6217–6227, doi:10.5194/acp-9-6217-2009, 2009.

Wang, Y., McElroy, M. B., Munger, J. W., Hao, J., Ma, H., Nielsen, C. P., and Chen, Y.: Variations of O_3 and CO in summertime at a rural site near Beijing, Atmos. Chem. Phys., 8, 6355–6363, doi:10.5194/acp-8-6355-2008, 2008.

Wang, Y., Zhang, Y., Hao, J., and Luo, M.: Seasonal and spatial variability of surface ozone over China: contributions from background and domestic pollution, Atmos. Chem. Phys., 11, 3511–3525, doi:10.5194/acp-11-3511-2011, 2011.

Wang, Z. F., Li, J., Wang, X. Q., Pochanart, P., and Akimoto, H.: Modeling of regional high ozone episode observed at two mountain sites (Mt. Tai and Huang) in East China, J. Atmos. Chem., 55, 253–272, doi:10.1007/S10874-006-9038-6, 2006.

Webster, P. J., Magana, V. O., Palmer, T. N., Shukla, J., Tomas, R. A., Yanai, M., and Yasunari, T.: Monsoons: processes, predictability, and the prospects for prediction, J. Geophys. Res., 103, 14451–14510, doi:10.1029/97JC02719, 1998.

Wiedinmyer, C., Sakulyanontvittaya, T., and Guenther, A.: MEGAN FORTRAN Code V2.04 User Guide, available at: http://acd.ucar.edu/~guenther/MEGAN/MEGAN.htm (last access: 31 January 2014), 2007.

Wild, O., Zhu, X., and Prather, M. J.: Fast-j: Accurate simulation of in- and below-cloud photolysis in tropospheric chemical models, J. Atmos. Chem., 37, 245–282, doi:10.1023/A:1006415919030, 2000.

Wu, S. L., Mickley, L. J., Leibensperger, E. M., Jacob, D. J., Rind, D., and Streets, D. G.: Effects of 2000–2050 global change on ozone air quality in the United States, J. Geophys. Res., 113, D06302, doi:10.1029/2007JD008917, 2008.

Yamaji, K., Ohara, T., Uno, I., Tanimoto, H., Kurokawa, J., and Akimoto, H.: Analysis of the seasonal variation of ozone in the boundary layer in East Asia using the Community Multi-scale Air Quality model: what controls surface ozone levels over Japan?, Atmos. Environ., 40, 1856–1868, doi:10.1016/j.atmosenv.2005.10.067, 2006.

Yan, P., Li, X., Luo, C., Xu, X., Xiang, R., Ding, G., Tang, J., Wang, M., and Yu, X.: Observational analysis of surface O_3, NO_x, and SO_2 in China, Appl. Meteor., 8, 53–61, 1997 (in Chinese).

Yan, P., Wang, M., Cheng, H., and Zhou, X. J.: Distributions and variations of surface ozone in Changshu, Yangtze Delta region, Acta Metallurgica Sinica, 17, 205–217, 2003.

Yang, G., Fan, S., Tang, J., Jin, S., and Meng, Z.: Characteristic of surface ozone concentrations at Lin'an, Res. Environ. Sci., 21, 31–35, 2008 (in Chinese).

Ye, D. Z.: Some Characteristics of the Summer Circulation over the Qinghai-Xizang (Tibet) Plateau and its neighborhood, B. Am. Meteorol. Soc., 62, 14–19, doi:10.1175/1520-0477(1981)062<0014:Scotsc>2.0.Co;2, 1981.

Yienger, J. J. and Levy, H.: Empirical-Model of Global Soil-Biogenic Nox Emissions, J. Geophys. Res., 100, 11447–11464, doi:10.1029/95JD00370, 1995.

Zhang, Y. H., Hu, M., Zhong, L. J., Wiedensohler, A., Liu, S. C., Andreae, M. O., Wang, W., and Fan, S. J.: Regional integrated experiments on air quality over Pearl River Delta 2004 (PRIDE-PRD2004): overview, Atmos. Environ., 42, 6157–6173, doi:10.1016/J.Atmosenv.2008.03.025, 2008.

Zhao, C., Wang, Y., Yang, Q., Fu, R., Cunnold, D., and Choi, Y.: Impact of East Asian summer monsoon on the air quality over China: view from space, J. Geophys. Res., 115, D09301, doi:10.1029/2009JD012745, 2010.

Zhou, D., Ding, A., Mao, H., Fu, C., Wang, T., Chan, L. Y., Ding, K., Zhang, Y., Liu, J., Lu, A., and Hao, N.: Impacts of the East Asian monsoon on lower tropospheric ozone over coastal South China, Environ. Res. Lett., 8, 044011, doi:10.1088/1748-9326/8/4/044011, 2013.

Zhou, L. T. and Huang, R. H.: Interdecadal variability of summer rainfall in Northwest China and its possible causes, Int. J. Climatol., 30, 549–557, doi:10.1002/joc.1923, 2010.

Zhu, J., Liao, H., and Li, J.: Increases in aerosol concentrations over eastern China due to the decadal-scale weakening of the East Asian summer monsoon, Geophys. Res. Lett., 39, L09809, doi:10.1029/2012GL051428, 2012.

Table 1. The composite analyses of horizontal and vertical fluxes of O_3 (Tg season^{-1}) for the selected box of (85–120° E, 20–46° N, the surface to 250 hPa) based on simulations O3_TOT and O3_TB. The values are averaged over the five weakest (1988, 1989, 1996, 1998, and 2003) and five strongest monsoon years (1990, 1994, 1997, 2002, and 2006), and the differences are calculated as (weakest–strongest). For horizontal fluxes, positive values indicate eastward or northward transport and negative values indicate westward or southward transport. For vertical fluxes, positive values indicate upward transport.

Side of the selected box	O_3_TOT			O_3_TB		
	Weakest	Strongest	Difference	Weakest	Strongest	Difference
Horizontal mass fluxes						
West	+83.7	+83.8	−0.1	+78.8	+78.9	−0.1
East	+106.5	+93.5	+12.9	+84.1	+73.1	+11.0
South	+13.4	+9.2	+4.2	+13.8	+10.5	+3.3
North	−19.3	−13.7	−5.5	−20.0	−15.0	−5.0
Vertical mass fluxes						
Top	+22.1	+20.7	+1.4	+16.5	+15.5	+1.0

ACPD
14, 3269–3300, 2014

Impacts of the East Asian summer monsoon on interannual variations

Y. Yang et al.

Title Page
Abstract | Introduction
Conclusions | References
Tables | Figures
|◀ | ▶|
◀ | ▶
Back | Close
Full Screen / Esc
Printer-friendly Version
Interactive Discussion

(a) O_3 Conc. (ppbv)

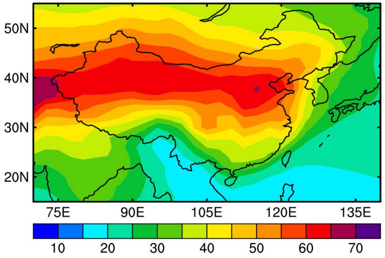

(b) MAD (ppbv)

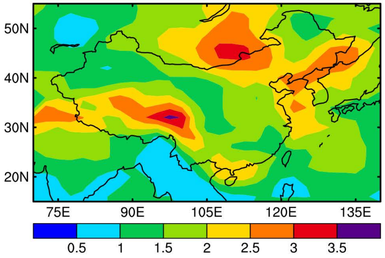

(c) APDM (%)

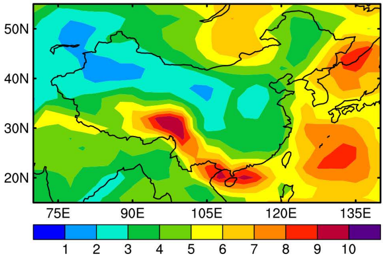

Fig. 1. (a) Simulated JJA surface-layer O_3 concentrations (ppbv) that are averaged over years 1986–2006 of simulation O3_TOT. **(b)** Mean absolute deviation (MAD, ppbv) and **(c)** absolute percent departure from the mean (APDM, %) calculated with 1986–2006 simulation of O_3 in O3_TOT.

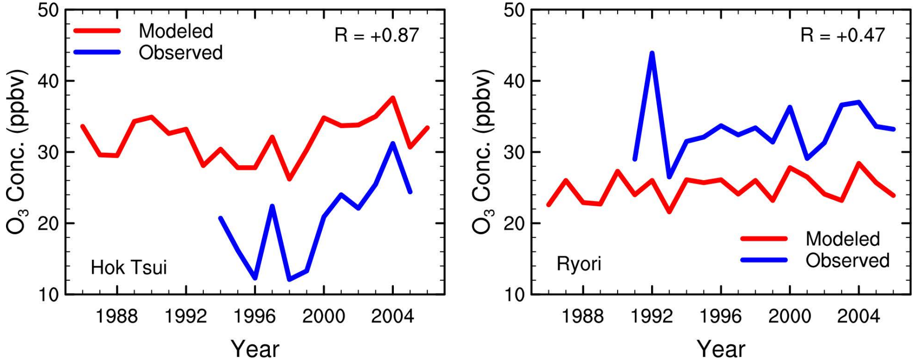

Fig. 2. Comparisons of observed and simulated JJA mean surface-layer O_3 concentrations at Hok Tsui (22°13′ N, 114°15′ E) in Hong Kong (left) and Ryori (39°03′ N, 144°82′ E) in Japan (right). Correlation coefficient between simulations and observations is shown at top right corner of each panel, which is calculated over the time period with observations available.

Title Page
Abstract | Introduction
Conclusions | References
Tables | Figures
◀▎ | ▶▎
◀ | ▶
Back | Close
Full Screen / Esc
Printer-friendly Version
Interactive Discussion

(a) EASMI & Surface O_3 Conc.

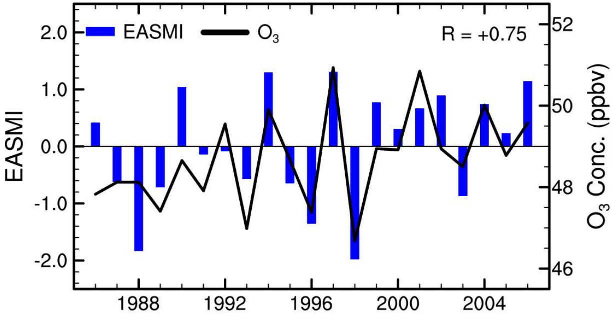

(b) Corr. EASMI & Surface O_3 Conc.

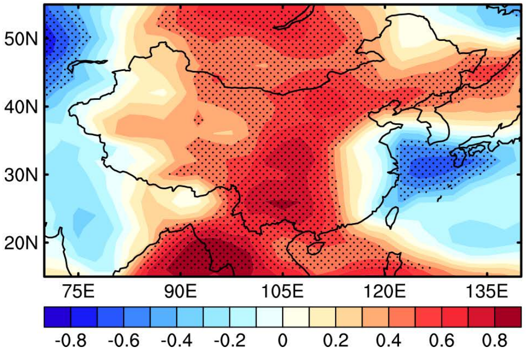

Fig. 3. (a) The normalized time series of EASMI (blue bars, left *y* axis) and the simulated JJA surface-layer O_3 concentrations (black line, right *y* axis, ppbv) averaged over China for years of 1986–2006. **(b)** Spatial distribution of the correlation coefficients between the EASMI and the JJA surface-layer O_3 concentrations. The dotted areas indicate statistical significance with 95 % confidence from a two-tailed Student's *t* test. The EASMI are calculated using the GEOS-4 assimilated meteorological data.

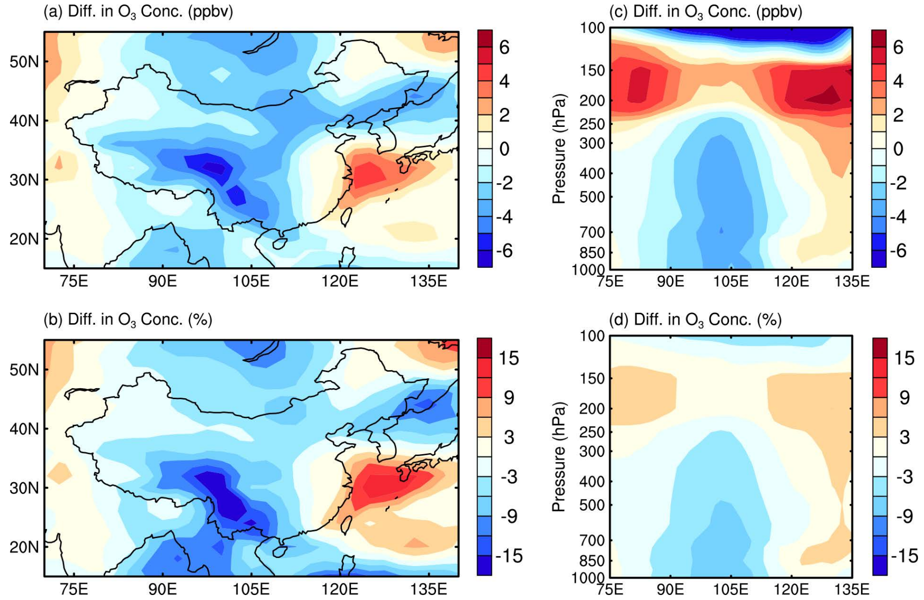

Fig. 4. Horizontal distributions of **(a)** absolute and **(b)** percentage differences in JJA surface-layer O_3 concentrations between the five weakest and strongest EASM years (weakest–strongest). Pressure-longitude cross sections averaged over 20–46° N for **(c)** absolute and **(d)** percentage differences in JJA O_3 concentrations between the five weakest and strongest EASM years (weakest–strongest). Results are from simulation O3_TOT and unit is shown on top of each panel.

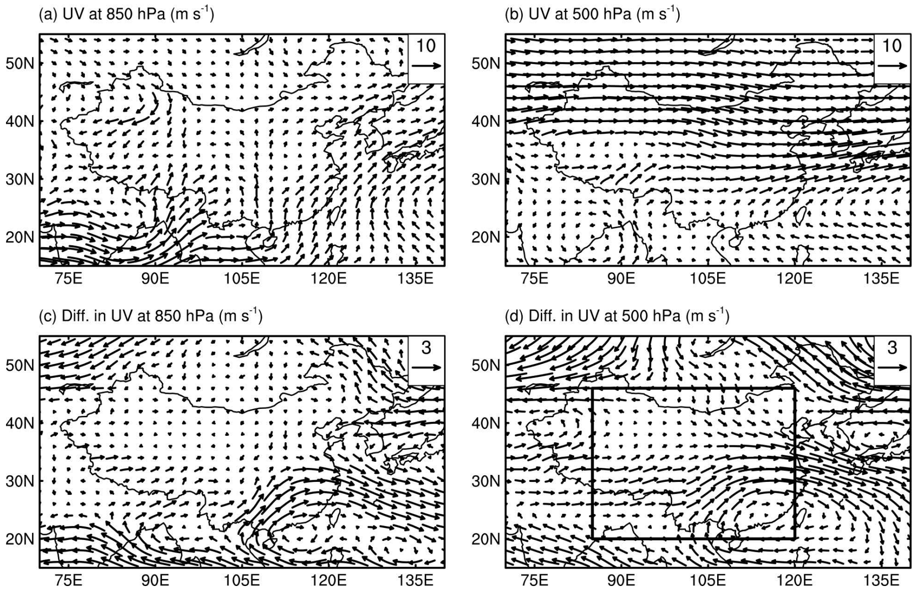

Fig. 5. The JJA mean horizontal winds at **(a)** 850 hPa and **(b)** 500 hPa averaged over 1986–2006. The composite differences in horizontal winds between the five weakest and strongest EASM years (weakest–strongest) at **(c)** 850 hPa and **(d)** 500 hPa. Horizontal winds are from the GEOS-4 assimilated meteorological data. Unit is shown on top of each panel. The location of box (85–120° E, 20–46° N, the surface to 250 hPa) selected to capture the features of transboundary O_3 transport is also shown in **(d)**.

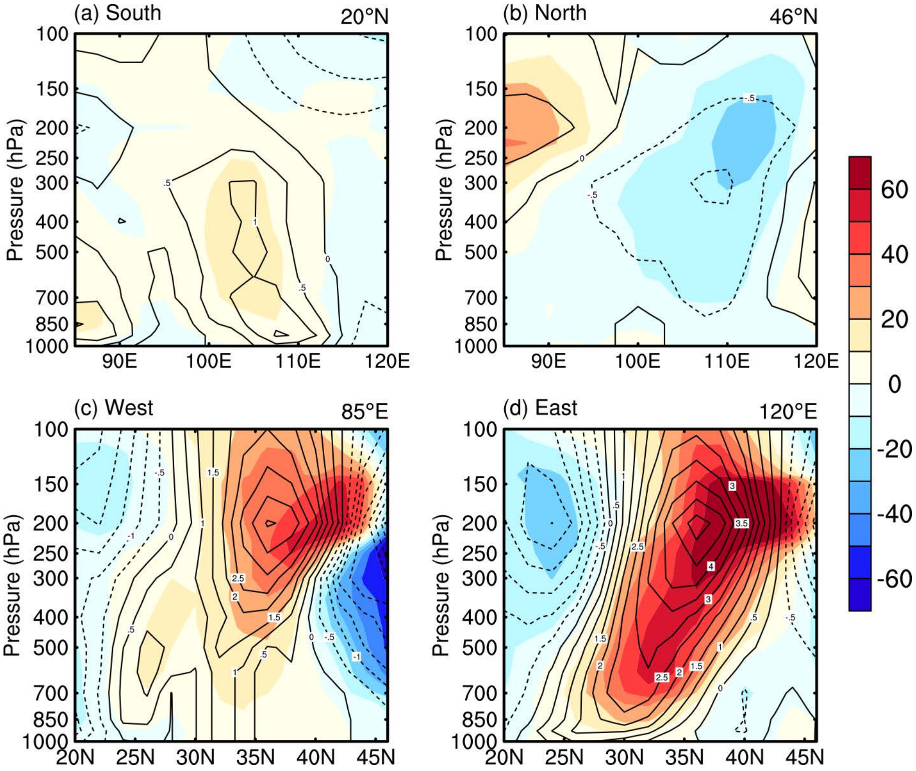

Fig. 6. The composite differences in horizontal O_3 fluxes (shades, $kg\,s^{-1}$) and winds (contours, $m\,s^{-1}$) at **(a)** south, **(b)** north, **(c)** west, and **(d)** east boundaries of the selected box of (85–120° E, 20–46° N, the surface to 250 hPa) between the five weakest and strongest EASM years (weakest–strongest). Fluxes and winds that are eastward or northward are positive, and those that are westward and southward are negative. Mass fluxes are from simulation O3_TOT. Longitudinal and meridional winds are from the GEOS-4 assimilated meteorological data.

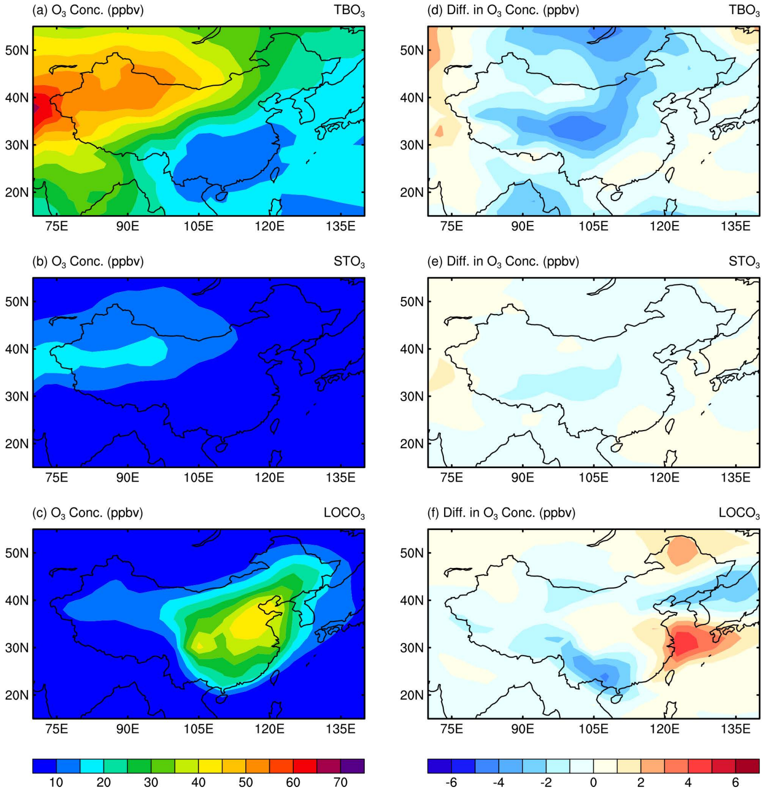

Fig. 7. The JJA surface-layer O_3 concentrations (ppbv) from **(a)** simulation O3_TB (referred to as TBO_3), **(b)** simulation O3_ST (referred to as STO_3), and **(c)** simulation O3_TOT minus simulation O3_TB (referred to as $LOCO_3$). Panels **(a)**, **(b)**, and **(c)** are the averages over 1986–2006. Panels **(d)**, **(e)**, and **(f)** are the composite differences (ppbv) in TBO_3, STO_3, and $LOCO_3$, respectively, between the five weakest and strongest EASM years (weakest–strongest).

Title Page
Abstract
Introduction
Conclusions
References
Tables
Figures
◀|
|▶
◀
▶
Back
Close
Full Screen / Esc
Printer-friendly Version
Interactive Discussion

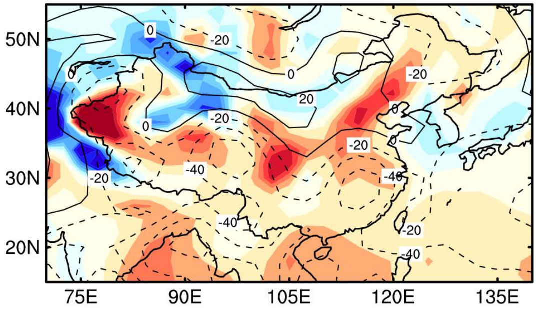

(a) OMEGA & O_3 vertical mass flux at 500 hPa

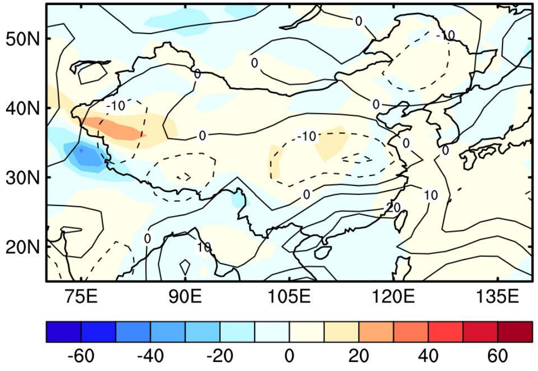

(b) Diff. in OMEGA & O_3 vertical mass flux at 500 hPa

Fig. 8. (a) The spatial distributions of JJA mean vertical wind velocity (contours, $\mathrm{Pa\,s^{-1}} \times 1000$) and simulated upward mass flux of O_3 (shades, $\mathrm{kg\,s^{-1}}$) averaged over 1986–2006. **(b)** The composite differences in vertical wind (contours, $\mathrm{Pa\,s^{-1}} \times 1000$) and simulated upward mass flux of O_3 (shades, $\mathrm{kg\,s^{-1}}$) between the five weakest and strongest EASM years (weakest–strongest). Vertical winds are from the NCEP/NACR reanalysis data.

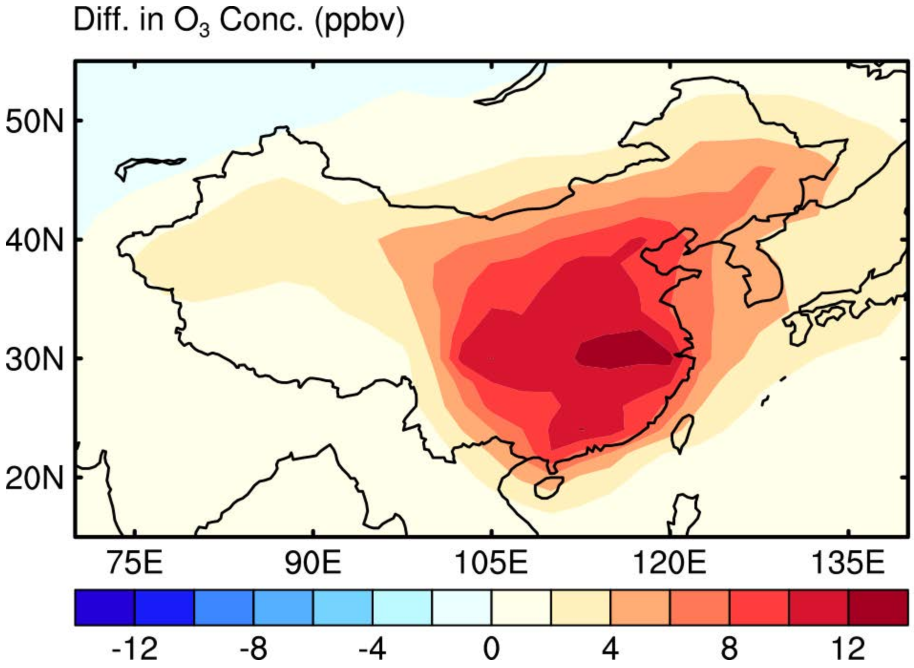

Fig. 9. The changes in simulated JJA surface-layer O_3 concentrations (ppbv) owing to the changes in anthropogenic emissions of O_3 precursors over 1986–2006, based on simulations of O3_EMIS.